occurred in the same places and wind strengths were approximately the same. This is because the main differences in topography resolved at T21 and T42 occur in the altitude range 10–15 km, where meridional winds are low as it is the transition zone between the upper and lower branches of the Hadley cell (Fig. 2). Over a range of surface drag parameters the minimum width of WBCs were ~15° in longitude. Although T21 resolution was adequate to resolve this, it was suspected that it may not have been enough to resolve the jet's core. We discovered, however, that the wind strengths were similar in runs at both T42 and T21 resolution (Fig. 2).

On Mars, bright depositional dust streaks observed at middle to low latitudes are believed to form in late southern summer and autumn[14–16], and are thought to be representative of global scale winds[3] during these times. The orientation of these streaks, when averaged over 5° × 5° cells, imply north—south wind flow, and are especially coherent at 40–50° W (ref. 17), which is consistent with the longitude and direction of the Tharsis WBC produced in a model simulation during southern summer (Fig. 1*a*). In addition, Haberle *et al.*[18], when comparing a one-dimensional boundary layer model with winds inferred from measurements taken during the entry of the Viking Lander 1 probe (at 48° W, 22° N) in early northern summer, found large discrepancies in wind speeds and their rotation with height which would be explained by significant advection of cold fluid from the southeast. This result is consistent with the presence of WBCs.

Boundary current winds also advect cold fluid towards the equator from the winter tropics, which might lead to a temperature signal observable by future spacecraft missions. The SGCM produces a strong thermal signal near the surface (see Fig. 4), although its magnitude may be significantly larger than that actually observed because the model representations of boundary-layer processes (such as heat and momentum transfer) are very simple at present.

WBCs may have a crucial role to play in the generation of global or great dust storms, because dust raising is critically dependent on low-altitude wind strength[19], which in turn is the result of the superposition of winds caused by different forcing mechanisms[20]. This hypothesis is supported by the fact that large eastward-facing slopes in low latitudes are locations where global dust storms have commonly been seen to originate[21] and these locations are coincident with the WBCs in our model.

Finally, it should be noted that the large diurnal temperature variation on Mars[22] might cause a diurnal variation in the strength of the Hadley cell and hence in the strength of WBCs. Such effects are being investigated with a more sophisticated numerical model. □

Received 23 September 1993; accepted 4 January 1994.

1. Anderson, D. L. T. *Globl atmos. Res. Progm. Pubs Ser.* **23,** 317–355 (1980).
2. Esposito, P. *et al.* in *Mars* (eds Kieffer, H H., Jakosky, B. M., Snyder, C. W. & Matthews, M. S.) Ch. 7 (Arizona Univ. Press, Tucson, 1992).
3. Greeley, R., Skypeck, A. & Pollack, J. B., *J. geophys. Res.* **98,** 3183–3196 (1993).
4. Gill, A. E. *Atmosphere–Ocean Dynamics* 516–522 (Academic, San Diego, 1982).
5. Hoskins, B. J. & Simmons, A. J. *Quart. Jl. R. met. Soc.* **101,** 637–655 (1975).
6. Phillips, N. A. *J. Met.* **14,** 184–185 (1957).
7. *Atlas of Mars* (US geol. Surv. Topographic Ser. No. M 15M, Flagstaff, 1989).
8. Goody, R. & Belton, M. J. *Planet. Space Sci.* **15,** 247–256 (1967).
9. James, I. N. & Gray, L. J. *Q. Jl. R. met. Soc.* **112,** 1231–1250 (1986).
10. Haberle, R. M. *et al. J. geophys. Res.* **98,** 3093–3123 (1993).
11. Conrath, B. J. *et al. J. geophys. Res.* **78,** 4267–4278 (1973).
12. Lindzen, R. S. & Hou, A. Y. *J. atmos. Sci.* **45,** 2416–2427 (1988).
13. Jakosky, B. M. & Haberle, R. M. in *Mars* (eds Kieffer, H. H., Jakosky, B. M., Snyder, C. W. & Matthews, M. S.) Ch. 28 (Arizona Univ. Press, Tucson, 1992).
14. Greeley, R., Lancaster, N., Lee, S. & Thomas, P. in *Mars* (ed Kieffer, H. H., Jakosky, B. M., Snyder, C. W. & Matthews, M. S.) Ch. 22 (Arizona Univ. Press, Tucson, 1992).
15. Ward, A. W., Doyle, K. B., Helm, P. J., Weisman, M. K. & Witback, N. E. *J. geophys. Res.* **90,** 2038–2056 (1985).
16. Thomas, P., Ververka, J., Gineris, D. & Wang, L. *Icarus,* **60,** 161–179 (1984).
17. Kahn, R. A., Martin, T. Z., Zurek, R. W. & Lee, S. W. in *Mars* (eds Kieffer, H. H., Jakosky, B. M., Snyder, C. W. & Matthews, M. S.) 1042–1043 (Arizona Univ. Press, Tucson, 1992).
18. Haberle, R. M., Houben, H. C., Hertenstein, R. & Herdtle, T. *J. atmos. Sci.* **50,** 1544–1559 (1993).
19. Greeley, R., Leach, R., White, B., Iversen, J. & Pollack, J. *Geophys. Res. Lett.* **7,** 121–124 (1980).
20. Leovy, C. B., Zurek, R. W. & Pollack, J. B. *J. atmos. Sci.* **30,** 749–762 (1973).
21. Martin, L. J. & Zurek, R. W. *J. geophys. Res.* **98,** 3221–3246 (1993).
22. Martin, T. Z. *Icarus* **45,** 427–446 (1981).

Assessing the pyroclastic flow hazard at Vesuvius

Flavio Dobran*†, Augusto Neri†‡ & Micol Todesco§

* Department of Earth System Science, New York University, New York, New York 10003, USA
† Istituto Nazionale di Geofisica, Via di Vigna Murata 605, Rome, Italy
‡ GNV, § Dipartimento di Scienze della Terra, Università di Pisa, Via S. Maria 53, 56100 Pisa, Italy

In large eruptions, Vesuvius has generated catastrophic avalanches of tephra and hot gases, such as those that destroyed Pompei and Herculaneum in AD 79, and Torre del Greco and surrounding towns in 1631[1–12]. These avalanches (pyroclastic surges and flows) are produced from collapses of the eruptive column, and can travel at >100 m s^{-1}, with temperatures exceeding 800 °C. In 1944 Vesuvius ended its most recent cycle of activity, which had begun with the explosive eruption of 1631. Here we use numerical simulations to assess the hazards posed by the pyroclastic flows that are likely to accompany the onset of the next cycle of activity. We examine three different scales of eruption, and use vent conditions established by modelling magma ascent along the conduit[13,14]. Our results indicate that large- and medium-scale eruptions can produce complete destruction in the 7 km radius around the volcano (an area in which one million people live and work) in about 15 minutes or less, and that only small-scale eruptions can be arrested by the topographic relief of Monte Somma.

The Somma–Vesuvius complex has exhibited various types of activity over the past 35,000 yr (ref. 1). Large-scale plinian eruptions (Codola, Sarno, Basal, Greenish, Lagno Amendolare, Mercato, Avellino and Pompei) erupted several cubic kilometres of material and have occurred every few centuries to millennia, whereas medium-scale sub-plinian eruptions (AD 412 and 1631) have occurred every few centuries, with each erupting ~0.1 km^3 of material[15]. It appears that the smaller-scale strombolian and effusive events occurring every few decades normally follow the plinian and sub-plinian eruptions until the conduit closes, and that the plinian and sub-plinian eruptions occur from the closed-conduit states of the volcano[12]. A common feature of the plinian eruptions is that they were interrupted intermittently as a result of partial column collapses producing pyroclastic surges and flows[2,5], and ended with the interaction of magma with water from underground aquifers[2,9,16]. The plinian and sub-plinian eruptions from the Avellino eruption ~3,400 yr ago to AD 1631 are all characterized by the emission of highly differentiated magmas, trachytic or phonolitic in character[17,18]. The pumice-fall deposits of Avellino, Pompei and the AD 1631 eruptions consist of white phonolite at the base and grey tephritic phonolite at the top[11,19]. Some insight on the future activity of Vesuvius, and on its effects on the surrounding area, can be established from studies of its past behaviour and distribution of its products[19]. The results from this kind of study are, however, poorly constrained by thermodynamics, geophysics and thermofluid-dynamics, and a more precise assessment of the future behaviour of Vesuvius could be achieved by modelling the entire volcanic system[12].

The available volcanological and petrological data for Vesuvius have recently been used to model magma ascent during the AD 79 eruption[13,20]. Based on the magma composition, temperature and crystal content, location of magma chamber, and stratigraphy, this modelling yielded likely values of conduit diameter, gas–pyroclast pressure and velocity distributions as a function of the mass discharge rate. The gas–pyroclast conditions at the vent were subsequently used in a physical model of the volcanic column[14] to study pyroclastic flows caused by column collapses. This column model employs a subgrid-scale

turbulence model, and the thermo-fluid dynamics includes the dispersive pressure produced by solid-particle collisions modelled by kinetic theory. The flow above the vent is assumed to be axisymmetric, consisting of a single particle size, and involving water vapour that may mix with the temperature- and pressure-stratified atmosphere.

The magma ascent and volcanic column physical models[13,14], combined with different topographic profiles of Vesuvius, provide a state-of-the-art simulation of the temporal and spatial evolution of eruption columns and associated pyroclastic flows. The main limitation of this axisymmetric flow modelling, as well as of that used in previous volcanic column studies[21,22], is that it does not account for the presence of valleys along the slopes of the volcano where three-dimensional topographic effects may strongly control the propagation of pyroclastic flows. Field studies of volcanic deposits and direct observations, however, distinguish dense and less mobile pyroclastic flows from less dense and more mobile pyroclastic surges[23]. This distinction is usually based on textural features of pyroclastic deposits which the model cannot resolve because of the use of a single particle size, large computational grid sizes and short simulation times. The characteristics of the simulated gas–pyroclast dispersions suggest, however, that they may be associated more closely with the pyroclastic surges. Because of the absence of precise quantitative criteria for distinguishing flows from surges, these flows will thus be referred to as 'pyroclastic flows'.

The input data for magma ascent and volcanic column models are shown in Table 1 as a function of three different mass eruption rates representing three different scales of eruption. The large mass eruption rate represents the grey eruption phase of Vesuvius in AD 79 (ref. 10), whereas the medium mass eruption rate is typical of a sub-plinian event such as that of AD 1631. The small mass eruption rate is an order of magnitude smaller than the large discharge rate. The gas–pyroclast conditions at the vents reported in the table pertain to the AD 79 grey magma composition and crystal content[13,16,24], and to a dissolved water content of 2 wt%. This magma water content reflects the more recent data of 2.5 wt% (ref. 25) pertaining to the AD 79 grey eruption phase, but some simulations were also performed with a water content of 3.5 wt% as reported previously in the literature[10]. Except as described below, detailed variations in magma composition (which at Vesuvius are associated with different scales of eruptions) are not taken into account in the model to limit the number of parameters. The conduit lengths and associated magma chamber pressures in Table 1 reflect different locations of plinian (large) and sub-plinian (medium and small) magma chambers[8,12], whereas the conduit diameters were determined by assuming that the given mass eruption rates correspond to choked or maximum flow conditions at the exit of the vent[20]. The pyroclast size of 100 μm employed in computer simulations represents one of the more mobile parts of the flow, as larger pyroclasts tend to be deposited at shorter distances from the vent whereas the smaller ones tend to follow the ascending hot plumes forming above the collapsed portion of the column and above the pyroclastic flow[14,26,27].

The vent conditions in Table 1 produced collapsed volcanic columns which generate pyroclastic flows along the two investigated topographic profiles of Vesuvius (Figs 1 and 2). Topography A accounts for the southern slope of the volcano toward the Tyrrhenian Sea, whereas topography B represents the route

TABLE 1 Input data for magma ascent and volcanic column modelling

Scale of the eruption	Large	Medium	Small
Mass eruption rate (kg s $^{-1}$)	1.5×10^8	5.0×10^7	1.5×10^7
Conduit length (km)	5	3	3
Magma chamber pressure (MPa)	124.7	74.7	74.7
Magma chamber temperature (K)	1,123	1,123	1,123
Pyroclast size (μm)	100	100	100
Dissolved water content of magma (wt%)	2	2	2
Conduit diameter (m)	100	60	40
Gas velocity at the vent (m s $^{-1}$)	118	130	135
Pyroclast velocity at the vent (m s $^{-1}$)	110	115	116
Gas–pyroclast temperature at the vent (K)	1,123	1,123	1,123
Pressure at the vent (MPa)	1.3	0.96	0.65
Particle volumetric fraction at the vent	0.067	0.052	0.0365

The mass eruption rate conduit length, magma chamber pressure and temperature, pyroclast size after magma fragmentation, and the AD 79 grey magma composition, crystal and dissolved water content, form the input data for magma ascent modelling[13]. The conduit diameter, pyroclast size and volumetric fraction, and gas–pyroclast temperature, pressure and volocities at the vent were established from magma ascent modelling and form the input data for the volcanic column modelling.

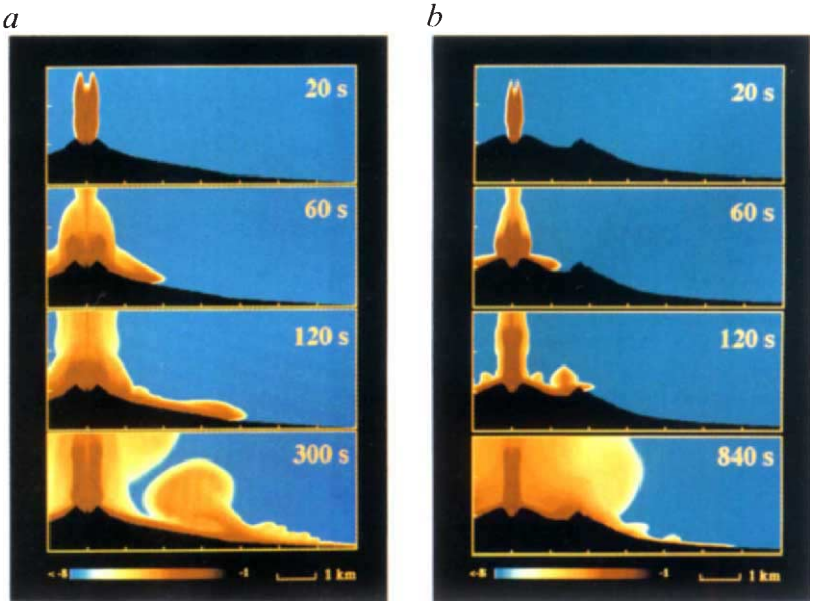

FIG. 1 *a*, Distribution of particle volumetric fraction at 20, 60, 120 and 300 s along the slope of Vesuvius toward the Tyrrhenian Sea (profile A) after the initiation of gas–particle discharge from a large-scale volcanic eruption of Vesuvius. *b*, Distribution of particle volumetric fraction at 20, 60, 120 and 840 s toward Somma Vesuviana (profile B) after the initiation of gas–particle discharge from a medium-scale volcanic eruption of Vesuvius. The red colour denotes very high, and the blue colour very low, particle volumetric fractions. The numbers on the colour scale at the bottom of the figures represent exponents to the base 10.

over Monte Somma towards the north in the direction of Somma Vesuviana. Figure 1*a* illustrates the evolution in time of the distribution of particle volumetric fraction of the large-scale eruption along the topography A. At ~20 s after the beginning of the eruption, the volcanic column reaches a height of ~3 km above the vent. Thereafter it begins to spread radially due to the loss of vertical momentum, and collapses to form a pyroclastic flow while a low-density plume rises above the collapsed portion of the column. At 60 s, the ground-hugging flow reaches a distance of ~2 km from the vent. At 120 s, the flow reaches a distance of 4 km, and at 300 s, it enters the Tyrrhenian Sea 7 km away from the vent. The results from computer simulations employing topography B (Fig. 1*b*) show that the morphological barrier of Monte Somma cannot stop the propagation of such a pyroclastic flow on the northern slope. By 300 s, a large-scale volcanic event in the vesuvian area is thus capable of destroying completely all the surrounding towns in the vicinity. The effect of Monte Somma on the pyroclastic flow propagation of a medium-scale eruption is shown in Fig. 1*b* by a sequence of time frames, demonstrating that even in this case the flow is not arrested and that it reaches a distance of ~6 km in 1,000 s. As seen in Fig. 1*a*, the break-in-slope of the volcano at ~3.5 km from the vent in the direction of the Tyrrhenian Sea produces a rising cloud (phoenix or co-ignimbrite column[14]) above the flow which subsequently merges with the collapsing and rising portions of the main column, and begins forming a large inward-necking volcanic plume. The Monte Somma relief shown in Fig. 1*b* produces an earlier development of the phoenix column (at ~1.2 km from the vent) beyond which a small pyroclastic flow propagates along the northern slope. Computer simulations of pyroclastic flows were not carried out beyond the 7-km radius from the vent in order to keep the calculations at a manageable level.

BOX 1 The AD 79 and 1631 eruptions of Vesuvius

The AD 79 Pompei eruption of Vesuvius started at about 13:00 on 24 August with the formation of a plinian column that was preceded by a phreatomagmatic opening phase. For the following seven hours, a phonolitic magma (white pumice) was ejected. At about 20:00 on the same day, the magma composition changed to tephritic phonolite (grey pumice), and after 01:00 on 25 August several pyroclastic surges and flows occurred, some of which were directly responsible for the destruction of Herculaneum and Pompei where 2,000 people were killed[1,3,5,7,10]. The Pompei eruption discharged ~4 km^3 of dense rock equivalent[5]. The AD 1631 eruption of Vesuvius was the most destructive event in the recent history of this volcano[11]. On 16 December 1631 at 06:30, the eruption started with the ejection of gas and ash, and by 10:00 it produced a plinian column. Between 19:00 and 22:00 on the same day, the eruption produced a succession of seismic shocks, and by 02:00 on 17 December a glowing cloud was seen issuing from the summit crater, flowing into the valley between the cone of Vesuvius and Monte Somma. During the night, lahars were also seen coming down from the northern slopes of Monte Somma, devastating the land around Ottaviano. At 11:00 a violent earthquake occurred and the central crater was seen discharging ash, gas and stones, which poured down the slopes of the cone of Vesuvius. These pyroclastic flows descended from the mountain in lobes and destroyed Torre del Greco and Torre Annunziata, 6 and 7 km from the crater, respectively. The eruption produced decapitation of the cone by ~500 m and ~4,000 deaths, primarily because of the pyroclastic flows. Extensive destruction was suffered by Ottaviano, Massa di Somma, San Sebastiano, San Giorgio and other places, and ~500 km^2 were covered by ash which destroyed crops, vineyards and cattle. □

On the basis of these results, an estimate of the pyroclastic flow hazard at Vesuvius can be made in terms of the different scales of the eruption, topographies A and B, and distances reached by the flow at different times (Fig. 2). As indicated above, the flow from a large-scale eruption cannot be stopped by any morphological barrier surrounding the volcano, and the effect of Monte Somma is only to retard the flow arrival times at sites distant from the vent (Fig. 2*a*). For a medium-scale volcanic event this flow retardation is more pronounced and is approximately twice as large as that of a large-scale eruption (Fig. 2*b*). The pyroclastic flow from a small-scale eruption also reaches the Tyrrhenian Sea at ~1,000 s but is arrested by Monte Somma (Fig. 2*c*). The computer simulations for a topography toward Ottaviano also demonstrate that pyroclastic flows from small-scale eruptions are arrested by Monte Somma. It is necessary to stress, however, that on the southern slopes of the volcano even small-scale eruptions can produce pyroclastic flows which reach the Tyrrhenian Sea, and which would produce localized destruction and panic among the population. When the computer simulations were performed with 3.5 wt% of dissolved water in the magma and for topography A, it was also found that the columns collapsed, but that the flows required slightly

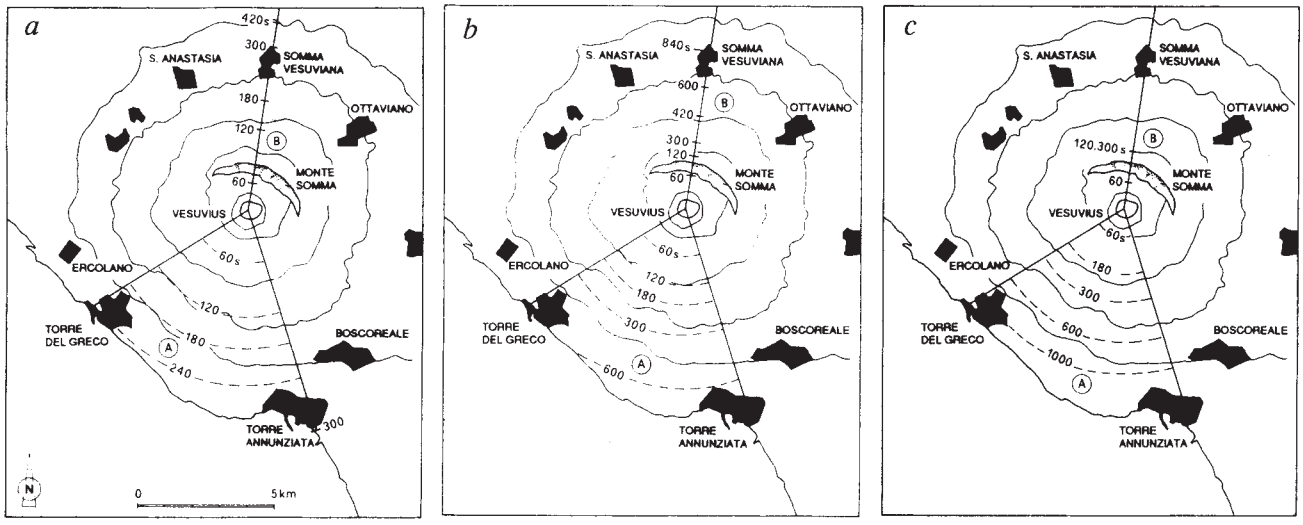

FIG. 2 Arrival time(s) of pyroclastic flows at different distances from the vent, for large- (*a*), medium- (*b*), and small-scale (*c*) eruptions, and topographies A and B in the directions of Tyrrhenian Sea and Somma Vesuviana, respectively. Note that the pyroclastic flows from all eruptions reach the Tyrrhenian Sea, and that only the flow from the small-scale eruption is arrested by Monte Somma. The hazard can be assessed by combining this information with the amount of material deposited, which can be derived from Fig. 1.

longer times to reach the Tyrrhenian Sea than the flows produced with 2 wt% of dissolved water in magma.

The results from computer simulations are consistent with the volcanological evidence of the pyroclastic flows and surges during the AD 79 and 1631 eruptions of Vesuvius[5,10,11]. In AD 79, the pyroclastic flows and surges reached the Tyrrhenian Sea in few minutes; a surge reached Somma Vesuviana to the north and Ottaviano to the northeast of Monte Somma. These pyroclastic flows and surges are generally associated with the partial collapses of the column produced by the changing conditions at the vent during the withdrawal of grey magma from magma chamber. According to a previous interpretation of the AD 79 eruption at Vesuvius[5], the main thrusting part of the column (the 'jet') extended ~3 km above the crater, only the jet part of the column collapsed during pyroclastic flow and surge productions, and the time interval between generations of some surges lasted only few minutes. These considerations are also consistent with our computer simulations. The pyroclastic flows and surges during the sub-plinian eruption of Vesuvius in AD 1631 also reached the Tyrrhenian Sea as predicted by our computer simulations for a medium-scale eruption. During the AD 79 eruption, pyroclastic flows and surges were produced only at later stages of the grey magma eruption phase[5,7]. To verify the effects of changing magma composition on the column collapse, we simulated the magma ascent and volcanic column for the white magma composition and 4.7 wt% of dissolved water in magma[5], followed by the emission from the same vent diameter of grey magma composition containing 3.5 wt% of dissolved water. This initially produced a plinian column, but with the emission of the grey magma the column exhibited partial collapses, implying that our simulations of pyroclastic flows at Vesuvius reflect the later stage of the grey magma eruption phase.

It should be noted that the predicted pyroclastic flow and surge distributions in the vesuvian area assume axisymmetric flow conditions and one granulometric particle size class. This implies that in reality these simulations should underestimate the maximum potential hazard due to these flows. The real flows are directed along preferential directions determined by local topography, and different sizes of pyroclasts will produce different mobilities, implying that surges, but not flows, may cross high reliefs as happened in the AD 79 eruption. Moreover, the presence of prevailing winds during eruptions can affect the column stability and also direct pyroclastic flows along preferred directions. These computer simulations of pyroclastic flows for the first time illustrate the timescales associated with this type of volcanic hazard in the vesuvian area. These simulations also indicate that future explosive eruptions at Vesuvius will have catastrophic effects for several hundred thousand people who live along its slopes, unless effective evacuation plans and new roads are built, and people begin depopulating the area. A proper way to assess the future volcanic hazard in this area is to develop a Global Volcanic Simulator for Vesuvius[12,28], based on interdisciplinary data and modelling all relevant physical processes in the volcanic complex. The simulator could be used to reconstruct more accurately past volcanic events at Vesuvius, forecast future eruptions, establish new safety codes for building and road construction, determine the best evacuation routes and educate the local population by dramatizing the impending danger of the sleeping giant. □

Received 24 August; accepted 3 December 1993.

1. Lirer, L., Pescatore, T., Booth, B. & Walker, G. P. L. *Geol. Soc. Am. Bull.* **84,** 759–772 (1973).
2. Sheridan, M. F., Barberi, F., Rosi, M. & Santacroce, R. *Nature* **289,** 282–285 (1981).
3. Sigurdsson, H., Cashdollar, S. & Sparks, R. S. J. *Am. J. Archeol.* **86,** 39–51 (1982).
4. Santacroce, R. *J. Volcan. geotherm. Res.* **17,** 237–248 (1983).
5. Sigurdsson, H., Carey, S., Cornell, W. & Pescatore, T. *Nat. Geogr. Res.* **1,** 332–387 (1985).
6. Arnó, V. *et al.* in *Somma–Vesuvius* (ed. Santacroce, R.) Vol. 114, 53–103 (CNR Quaderni, Roma, 1987).
7. Carey, S. & Sigurdsson, H. *Geol. Soc. Am. Bull.* **99,** 303–314 (1987).
8. Santacroce, R. (ed.) *Somma–Vesuvius* Vol. 114 (CNR Quaderni, Roma, 1987).
9. Barberi, F. *et al. J. Volcan. geotherm. Res.* **38,** 287–307 (1989).
10. Sigurdsson, H., Cornell, W. & Carey, S. *Nature* **345,** 519–521 (1990).
11. Rosi, M., Principe, C. & Vecci, R. *J. Volcan. geotherm. Res.* (in the press).
12. Dobran, F. *Global Volcanic Simulation of Vesuvius* (Giardini, Pisa, 1993).
13. Papale, P. & Dobran, F. *J. Volcan. geotherm. Res.* **58,** 101–132 (1993).
14. Dobran, F., Neri, A. & Macedonio, G. *J. geophys. Res.* **98,** 4231–4259 (1993).
15. Macedonio, G., Pareschi, M. T. & Santacroce, R. *J. Volcan. geotherm. Res.* **40,** 327–342 (1990).
16. Barberi, F., Navarro, J. M., Rosi, M., Santacroce, R. & Sbrana, A. *Rend. Soc. Ital. Miner. Petrol.* **43,** 901–926 (1988).
17. Civetta, L., Galati, R. & Santacroce, R. *Bull. volcan.* **53,** 287–300 (1991).
18. Civetta, L. & Santacroce, R. *Acta vulcan.* **2,** 147–159 (1992).
19. Rosi, M., Santacroce, R. & Sheridan, M. in *Somma–Vesuvius* (ed. Santacroce, R.) Vol. 114, 197–220 (CNR Quaderni, Roma, 1987).
20. Dobran, F. *J. volcan. geotherm. Res.* **49,** 285–311 (1992).
21. Wohletz, K. H., McGetchin, T. R., Sandford, M. T. & Jones, E. M. *J. geophys. Res.* **89,** 8269–8285 (1984).
22. Valentine, G. A., Wohletz, K. H. & Kieffer, S. W. *Geol. Soc. Am. Bull.* **104,** 154–165 (1992).
23. Cas, R. A. F. & Wright, J. V. *Volcanic Successions: Modern and Ancient* (Chapman & Hall, London, 1987).
24. Barberi, F. *et al. Bull. Volcan.* **44,** 295–315 (1981).
25. Cioni, R. *et al.* (abstr.) Annual Meeting CNR–Gruppo Nazionale per la Vulcanologia, 8–10 June, Rome (Giardini, Pisa, 1993).
26. Neri, A. & Dobran, F. *J. geophys. Res.* (submitted).
27. Giordano, G. & Dobran, F. *J. Volcan. geotherm. Res.* (in the press).
28. Dobran, F. *Int. Symp. on Large Explosive Eruptions* (Accademia Nazionale dei Lincei, 24–25 May, Rome (1993).

Parasitism, mutation accumulation and the maintenance of sex

R. Stephen Howard & Curtis M. Lively

Department of Biology, Indiana University, Bloomington, Indiana 47405, USA

Two classes of models attempt to explain why obligate parthenogenesis only rarely replaces sexual reproduction in natural populations, in spite of the apparent reproductive advantage that parthenogens gain by producing only female offspring[1]. The mutation-accumulation models suggest that sex is adaptive because it purges the genome of harmful recurrent mutations[2,3]. The ecological genetic models postulate that sex is adaptive in variable environments, particularly when the relevant variation is generated by coevolutionary interactions with parasites[4–7]. Both of these models have considerable merit, but would seem to have limitations. The mutation-accumulation models require high rates of mutation[3,8]; the coevolutionary models require that parasites have severe fitness effects on their hosts[9]. In addition, parasites could select for clonal diversity and thereby erode any advantage that sex gains by producing variable progeny[10]. Here we consider the interaction between mutation accumulation and host–parasite coevolution. The results suggest that even moderate effects by parasites combined with reasonable rates of mutation could render sex evolutionarily stable against repeated invasion by clones.

The crux of the 'red queen' hypothesis is that there is time-lagged, frequency-dependent selection against common host genotypes[5–7]. Parasites are expected to evolve rapidly so as to infect disproportionately any genotype that becomes common, and thereby drive it down in frequency[11,12]. This sets up an oscillation in which parasite gene frequencies track the gene frequencies of their host. This kind of antagonistic coevolution could theoretically prevent the local fixation of any host genotype; but, to prevent the fixation of a clone with a twofold reproductive advantage, the direct effects of parasites would need to be severe[9], or there would have to be rank-order truncation selection against the most infected individuals[13].

Even with severe effects of parasites (for example, parasitic castration), it would seem that clones would still have a reproductive advantage when rare. Such an advantage could easily explain the local coexistence of reproductively isolated sexual and parthenogenetic lines, but it leads to another potential problem. Repeated mutations to parthenogenetic reproduction would lead to the accumulation of clones; and assuming that